Trapped-Ion Quantum Logic Gates Based on Oscillating Magnetic Fields

C. Ospelkaus, C. E. Langer,* J. M. Amini, K. R. Brown, D. Leibfried, and D. J. Wineland

National Institute of Standards and Technology, 325 Broadway, Boulder, Colorado 80305, USA

Oscillating magnetic fields and field gradients can be used to implement single-qubit rotations and entangling multiqubit quantum gates for trapped-ion quantum information processing (QIP). With fields generated by currents in microfabricated surface-electrode traps, it should be possible to achieve gate speeds that are comparable to those of optically induced gates for realistic distances between the ion crystal and the electrode surface. Magnetic-field-mediated gates have the potential to significantly reduce the overhead in laser-beam control and motional-state initialization compared to current QIP experiments with trapped ions and will eliminate spontaneous scattering, a fundamental source of decoherence in laser-mediated gates.

Most current schemes for quantum information processing with trapped ions use laser-induced interactions to implement single-qubit rotations and entangling multiqubit gates by coupling the internal states of ions to their motion [1,2]. While these schemes have been successful in manipulating small numbers of ions, scaling up to larger register sizes and/or multiple quantum registers will require a large overhead in laser-beam power and control. Moreover, operation fidelities will eventually determine the necessary overhead for quantum error correction, making it desirable to minimize gate imperfections. For laser-induced gates, fidelities are currently limited by fluctuations of classical parameters, such as noise in laser-beam intensity at the ion positions. For gates induced by stimulated-Raman transitions, spontaneous emission poses an additional fundamental limit [3].

One possible approach to mitigate the overhead of laser-beam control replaces the precise timing of laser beams with the precise control of ion transport through stationary beams [4]. An alternative to laser-induced gates would be to use magnetic fields and their gradients to perform gate operations, thereby eliminating spontaneous-emission decoherence during operations. As discussed in [5–7], applying a static magnetic-field gradient provides qubit addressing and state coupling of motional and internal quantum states as required for two-ion entangling gates. Reference [4] also considered implementing multiqubit gates by transporting ions over a microfabricated static magnetic-field pattern. This takes advantage of the small length scales of microfabricated surface-electrode traps to realize strong oscillating magnetic-field gradients in the rest frame of the ion, and could thereby achieve competitive gate speeds [8].

Coupling between internal and motional states is particularly strong with laser beams (wavelength λ) where the length scale for field gradients is given by $\lambda/2\pi$. However, if current-carrying structures can be made small enough,

oscillating magnetic fields can also be used to implement this coupling [9], as in the $g - 2$ experiments of Dehmelt and co-workers [10]. In the context of coupled-spin Hamiltonian simulation, Ref. [11] discussed the use of circular coils in a surface array to implement these Hamiltonians with oscillating magnetic fields.

In this Letter, we discuss the implementation of single- and multiqubit logic gates with oscillating magnetic fields in the context of universal computation. We analyze gates based on $\sigma_\varphi \sigma_\varphi$ [12–14] and $\sigma_z \sigma_z$ [8,15] couplings, where σ_i are Pauli operators, and $\sigma_\varphi = \cos\varphi \sigma_x + \sin\varphi \sigma_y$. We also consider the integration of the field-producing conductors with the requirements for surface-electrode traps [16,17] and compare these gates with those implemented with laser beams. We give some numerical examples based on $^9\text{Be}^+$ qubits, but other ions will have comparable values.

We consider a string of N ions of mass m, aligned along the y axis. We assume the trap axes orthogonal to y are aligned along the x and z directions. Two internal states $|\uparrow\rangle$ and $|\downarrow\rangle$ of each ion compose a qubit with transition frequency ω_0. We choose the z axis as the quantization axis, provided by a static magnetic field $B_0 \vec{e}_z$. Let q_n be the displacement (along x or z) of ion n relative to its equilibrium position ($q_n = 0$). We write q_n in terms of normal modes with coordinates $\tilde{q}_j$ and frequencies ω_j: $q_n = \sum_j b_{j,n} \tilde{q}_j$ [18]. With $\tilde{q}_0^j := \sqrt{\hbar/(2m\omega_j)}$, we have $\tilde{q}_j = \tilde{q}_0^j(\hat{a}_j + \hat{a}_j^\dagger)$, where $\hat{a}_j^\dagger$ and $\hat{a}_j$ are normal-mode creation and annihilation operators. The interaction-free Hamiltonian for the qubit states and the motion can be written as $H_0 = \sum_n \frac{\hbar\omega_0}{2}\sigma_z^n + \sum_j \hbar\omega_j \hat{a}_j^\dagger \hat{a}_j$. An oscillating magnetic field $\vec{B}(q,t) = \vec{e}_x B_x + \vec{e}_z B_z = [\vec{e}_x(\tilde{B}_x + q\tilde{B}_x') + \vec{e}_z(\tilde{B}_z + q\tilde{B}_z')] \times \cos(\omega t + \varphi)$ couples the internal states and the motion. The interaction-picture magnetic dipole Hamiltonian for ion n in the rotating-wave approximation is given by

$$H_{I,n} = -\hbar e^{-i(\omega t + \varphi)}\left[(\Omega^x \sigma_+^n e^{i\omega_0 t} + \Omega^z \sigma_z^n) + \sum_j (\Omega_{j,n}^x \sigma_+^n e^{i\omega_0 t} + \Omega_{j,n}^z \sigma_z^n)(e^{-i\omega_j t}\hat{a}_j + e^{i\omega_j t}\hat{a}_j^\dagger)\right] + \text{H.c.} \qquad (1)$$

The Rabi frequencies are given by

$$\Omega^z = \frac{\tilde{B}_z}{4\hbar}(\mu_{z\uparrow\uparrow} - \mu_{z\downarrow\downarrow}), \qquad \Omega^x = \frac{\tilde{B}_x}{2\hbar}\mu_{x\downarrow\uparrow},$$

$$\Omega_{j,n}^z = \frac{b_{j,n}\tilde{q}_0^j \tilde{B}_z'}{4\hbar}(\mu_{z\uparrow\uparrow} - \mu_{z\downarrow\downarrow}), \qquad \Omega_{j,n}^x = \frac{b_{j,n}\tilde{q}_0^j \tilde{B}_x'}{2\hbar}\mu_{x\downarrow\uparrow}.$$

The matrix elements of an ion's magnetic moment $\vec{\mu}$ we write as $\mu_{x\downarrow\uparrow} = \langle\downarrow|\mu_x|\uparrow\rangle$, etc. The Ω^z term in (1) describes periodic changes in the energy of each ion qubit due to the oscillating z component of the magnetic field. The Ω^x term describes driven Rabi oscillations applied simultaneously to all ion-qubits ("carrier" transitions) if the driving field frequency is close to ω_0. Both terms implement global single-qubit rotations. We have neglected additional single-qubit terms in Eq. (1) proportional to the identity operator times $\mu_{z\uparrow\uparrow} + \mu_{z\downarrow\downarrow}$; for multiqubit gates described below, their effects can be eliminated with simple rotations.

The remaining terms in (1) describe simultaneous changes of internal and motional states and can therefore be used to implement multi-ion entangling gates. From the $\Omega_{j,n}^x$ term, we obtain spin-flip transitions simultaneous with the creation or annihilation of phonons in motional mode j (for $\omega \approx \omega_0 \pm \omega_j$). For a single ion, $\Omega_{j,n}^x$ is the Rabi flopping frequency for the first "blue and red sideband" transitions ($\omega = \omega_0 \pm \omega_j$). The $\Omega_{j,n}^z$ term, on the other hand, provides qubit-state-dependent excitation of motional mode j without simultaneous spin flips.

To implement multiqubit gates, we first consider an oscillating B_z field close to a normal-mode frequency ω_j ($\omega = \omega_j - \delta$), and keep only near-resonant terms in (1). Under the influence of this periodic force, the motional state of the ion follows a circular trajectory in phase space [8]. At $\tau = 2\pi/\delta$, the motional state has returned to the origin, and the propagator is

$$\mathcal{U}_{zz}(\tau) = \exp\left[\frac{2\pi i}{\delta^2}\left(\sum_n \Omega_{j,n}^z \sigma_z^n\right)^2\right]. \qquad (2)$$

For a two-ion "rocking" mode ($b_{j,1} = -b_{j,2}$) and the detuning $\delta/4 = \Omega_{j,n}^z$, we obtain a $\sigma_z\sigma_z$ phase gate equivalent to Refs. [8,15]. The $\sigma_z\sigma_z$ gate requires $\mu_{z\uparrow\uparrow} \neq \mu_{z\downarrow\downarrow}$ and can therefore not be directly applied to qubit states that are magnetic-field insensitive to first order, which is desirable for long coherence times [19,20]. However, with the use of efficient single-qubit rotations as discussed here, it is possible to temporarily transform from the field-independent qubit-state manifold and perform the gate.

The $\Omega_{j,n}^x$ term can be used to implement the $\sigma_\varphi\sigma_\varphi$ gate [12–14]. We can simultaneously apply two equal-amplitude B_x fields at frequencies detuned from the first blue and red sideband by δ ($\omega_{b,r} = \omega_0 \pm \omega_j \mp \delta$) with phases φ_b and φ_r, and keep only resonant multiqubit spin-flip terms. Again, at $\tau = 2\pi/\delta$, the motional mode has returned to its initial state, and the propagator is

$$\mathcal{U}_{\varphi\varphi}(\tau) = \exp\left[\frac{2\pi i}{\delta^2}\left(\sum_n \Omega_{j,n}^x \sigma_{\varphi_s}^n\right)^2\right], \qquad (3)$$

where $\varphi_s = (\varphi_b + \varphi_r)/2$. We thus obtain the equivalent propagator to the $\sigma_z\sigma_z$ gate, which now acts on the single-qubit eigenstates of $\sigma_{\varphi_s}^n$.

To estimate the coupling strengths, consider a current $I\vec{e}_y$ running through a thin straight wire located on the y axis. This produces a field $[-I\mu_0/(2\pi d)]\vec{e}_z$ and field gradients $\partial B_x/\partial z = \partial B_z/\partial x = I\mu_0/(2\pi d^2)$ at $(x, z) = (d, 0)$. For an ion located at these positions, Rabi frequencies for single-qubit rotations are therefore proportional to $1/d$, whereas Rabi frequencies for entangling gates scale as $\tilde{q}_0^j/d^2 \propto (m\omega_j)^{-1/2}d^{-2}$. As an example, for $^9\text{Be}^+$ and $\omega_j = 2\pi \times 5$ MHz, $\tilde{q}_0^j \approx 10$ nm, which is small compared to current values of ion-to-electrode distances d (25 to 100 μm). Therefore, significant off-resonant carrier excitation (Ω^x) and ac-Zeeman shifts would occur during multiqubit gates unless current geometries with a strong gradient and a small absolute value of the field are used.

We now examine possible current geometries compatible with surface-electrode traps. For single-qubit rotations, we require oscillating fields transverse to B_0. To implement the $\sigma_z\sigma_z$ multiqubit gate, the ions need to sample changes in B_z during their motion; for the $\sigma_\varphi\sigma_\varphi$ gate, the ions need to sample changes in B_x or B_y during motion. For either gate we desire $B_x = B_z = 0$ at the ions. Figure 1 shows how these requirements can be integrated in an example surface-electrode trap. The trapping potential of this "five-wire" surface trap [21] is provided by a central static potential electrode (a), two rf electrodes (b), additional static potential electrodes (c), (d), and segmented outer electrodes (e) providing confinement along y. The ion is trapped at the rf pseudopotential null line at a distance d_0 from the surface. The electrode dimensions
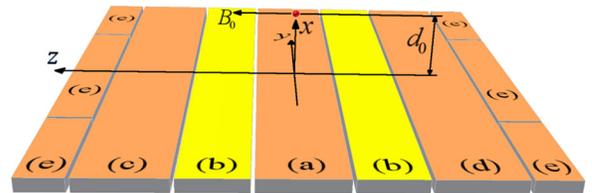

FIG. 1 (color online).   Example geometry for driving ion-qubit gates with oscillating magnetic fields produced by surface-electrode traps. The trap electrodes lie in the yz plane. The ion is assumed to be trapped at a distance d_0 above the trap plane. Oscillating currents in electrodes (a), (c), and (d) can be used to implement single-qubit rotations and entangling gates (see text). The electrode widths are $5/4d_0$ [(a),(c),(d)] and $39/40d_0$ [(b)]. We assume a uniform distribution of currents in the surface.

along z are chosen so that antiparallel currents $I(t) = \tilde{I}\cos(\omega t + \varphi)$ through electrodes (c) and (d) provide a field $\tilde{B}_x = 1.5 \times 10^{-7} I(t)/d_0$ T at the ion to implement rotations, where I and d_0 are expressed in amperes and meters, respectively. For $d_0 = 30$ μm and using the field-independent ^{9}Be$^+$ qubit ($B_0 = 12$ mT with $|\uparrow\rangle = |F = 1, m_F = 1\rangle$ and $|\downarrow\rangle = |F = 2, m_F = 0\rangle$ [20], $\mu_{x|\uparrow\rangle} = 0.48\mu_B$, where μ_B is the Bohr magneton), a carrier π pulse can be achieved in 1 μs with $\tilde{I} = 15$ mA. For multiqubit gates, an oscillating current $I(t)$ through the central conductor (a) produces a field $B_z(t)$ at the ion. Two currents $-2.5I(t)$ in conductors (c) and (d) produce a field $-B_z(t)$ at the ion, thereby nulling the field while all three currents provide field gradients $\partial B_x(t)/\partial z = \partial B_z(t)/\partial x = 2.5 \times 10^{-7} I(t)/d_0^2$ T/m for motional-state excitation and multiqubit gates. As an example, for the $\sigma_\varphi\sigma_\varphi$ gate consider the first-order field-insensitive ^{9}Be$^+$ qubit (see above) and $d_0 = 30$ μm. The gate implemented on a radial z "rocking" or COM (center-of-mass) mode with $\omega_j = 2\pi \times 5$ MHz could be realized in $\tau = 20$ μs with $\tilde{I} = 1.7$ A [$\tau \propto (m\omega_j)^{1/2}/(\partial B_x/\partial z)$]. For comparison, similar cw currents have been achieved in neutral atom magnetic chip traps of similar size. For the equivalent $\sigma_z\sigma_z$ gate, consider the ^{9}Be$^+$ states $|\uparrow\rangle = |F = 2, m_F = 2\rangle$ and $|\downarrow\rangle = |F = 2, m_F = 0\rangle$ ($\mu_{z|\uparrow\rangle} = -1.0\mu_B$; $\mu_{z|\downarrow\rangle} = 0.26\mu_B$), which can be reached from the field-independent qubit manifold with one microwave pulse. For a radial x rocking or COM mode, the gate can be realized in the same time with $\tilde{I} = 1.3$ A.

Practical implementation of these gates must account for a number of possible complications. Induced currents in neighboring trap electrodes will alter the magnetic fields and their gradients at the position of the ion. To estimate these effects as a function of frequency, we have performed finite-element numerical simulations of current flow in sample trap structures. The inset in Fig. 2 shows a U-shaped current loop, a geometry useful for single-qubit rotations. The center electrode and any surrounding trap electrodes are held at rf ground. The diagonal cuts in the outer plane serve to mimic the effect of the static potential control electrodes. Since the impedance of the circuit can change substantially over the considered frequency range, we have assumed that a fixed input power is dissipated in 6 μm thick gold conductors ($\rho = 2.44 \times 10^{-8}$ Ω m) at each frequency. Figure 2 shows the resulting magnetic field at a position $d_0 = 30$ μm above the surface, normalized to the dc result. For frequencies up to about 20 MHz (operating regime of a typical $\sigma_z\sigma_z$ gate), the resulting magnetic field is close to the dc value.

In a large-scale device with multiple zones, it will be desirable to avoid "crosstalk" between zones. By adding more alternating currents to the geometry, it may be possible to achieve field decay with a desired polynomial order. Alternatively, compensating currents could be applied in neighboring trap zones to cancel crosstalk. For gate durations longer than a motional period, two-qubit gates
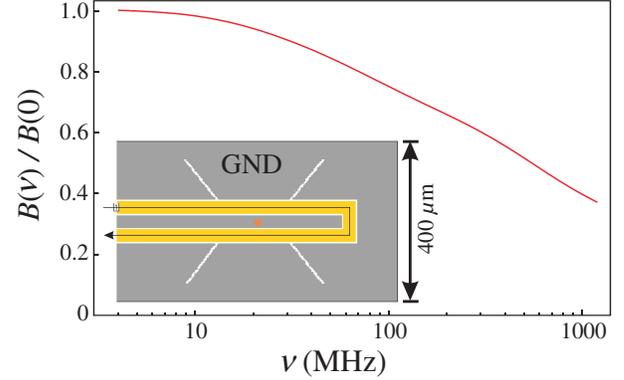

FIG. 2 (color online). Simulation of magnetic fields resulting from surface currents in an example trap structure, viewed from above. The figure shows the frequency dependence of the field 30 μm above the center of the trap for the U-shaped current loop shown in the inset.

will be effective only if the motional frequency is close to the gate-drive frequency. Therefore effects on ions in neighboring zones can be suppressed by confining them in potentials with different motional frequencies.

Moreover, the currents applied to the electrode structures will likely be accompanied by oscillating electric potentials. This is of particular importance for the $\sigma_z\sigma_z$ gate on a COM mode, where the resulting oscillating electric field couples directly to the motional mode. For the $\sigma_z\sigma_z$ example discussed above, the (state-dependent) magnetic force on an ion in $|F = 2, m_F = 2\rangle$ is equal to the (state-independent) electric force for an oscillating potential of 2.3 μV on electrode (a). Depending on the details of implementation and sources of electric fields, this effect can be compensated, because it yields only single-qubit phases, but these phases may be large and difficult to control. These effects are highly suppressed for $\sigma_z\sigma_z$ gates implemented on the rocking modes and the $\sigma_\varphi\sigma_\varphi$ gates.

Because of the strong field gradients desired for entangling gates, the ion will experience significant oscillating fields when displaced from the field null. To avoid off-resonant carrier excitations and ac-Zeeman shifts, it may be necessary to make the current through conductors (c) and (d) in Fig. 1 adjustable, or to include additional "B-field compensation" wires to null the oscillating magnetic field, in analogy to micromotion compensation in ion traps [22]. To estimate the effect of imperfect cancellation, we assume that the ions are located 200 nm away from the field null along z. For either gate, the oscillating field will cause single-qubit phases no larger than 43 mrad. These phases can be nulled by a suitable spin-echo sequence [8,23] and/or (for the $\sigma_\varphi\sigma_\varphi$ gate) by a smooth overall global pulse envelope, because they commute with the gate. Note that in the corresponding $\sigma_\varphi\sigma_\varphi$ laser gate, these off-resonant carrier excitations can also be avoided by placing the ions at the node of a standing-wave laser beam. However, due to the difficulty of locating the ions at a node, this gate has so far been realized only with

running wave beams, where off-resonant carrier excitations proportional to $\sigma_{\pi/2-\varphi}$ occur. These interactions do not commute with the gate and represent an important gate error [14] that is absent in the magnetic gate.

An important benefit of magnetic-field gates is their relative insensitivity to motional-state initialization. In laser-mediated multiqubit gates, it is usually necessary to initialize the ions very close to the motional ground state to avoid nonlinearity in the motional excitation. The extent of the motional ground-state wave function is on the order of 10 nm, typically just 1 order of magnitude smaller than the spatial structure of the laser beams, given by $\lambda/(2\pi)$. Therefore, the ions will experience different values of $\Omega_{j,n}^x$ and $\Omega_{j,n}^z$ due to higher-order terms in the driving fields when they occupy different excited motional states. For the magnetic-field gradient gates discussed here, the gate fidelity is insensitive to the initial motional state up to the point where the modes become anharmonic, as long as the field gradient is constant over the ion trajectory [as assumed in Eq. (1)]. Higher-order terms in the Rabi rates will be suppressed by a factor of $\approx (\tilde{q}_0^j/d_0)^2$ compared to the linear terms. This should allow for gate operation on ions that are only Doppler cooled, removing the need for near-ground-state cooling. Similarly, if ion motion is significantly excited during transfer in a multizone array, sympathetic Doppler cooling should be sufficient for high-fidelity gates. On the other hand, if ground-state cooling is desired, it can be implemented with the use of red-sideband transitions driven by oscillating magnetic-field gradients and optical pumping. This motional-state insensitivity might also permit gate durations smaller than a motional period [24] because much larger trajectories in phase space can be tolerated.

There are additional important practical differences between the $\sigma_\varphi \sigma_\varphi$ gate and the $\sigma_z \sigma_z$ gate. The latter operates at a frequency close to the relatively low motional frequencies, which will facilitate the generation of the required rf currents in a conductor structure. Also, the $\sigma_z \sigma_z$ gate can be readily applied to "optical" ion qubits where the two qubit states are, for example, S and D states as in Ca^+. The only requirement is that the two qubit states have different magnetic moments. The $\sigma_\varphi \sigma_\varphi$ gate, on the other hand, can be applied directly to first-order magnetic field-insensitive qubits and avoids the electric field excitation noted above. However, it would typically operate at a higher frequency of 1 to 15 GHz, corresponding to hyperfine splittings, which makes it technically more difficult to implement. Exceptions include qubits based on the low-field Zeeman states of a $2S_{1/2}$ level in an ion without nuclear spin.

In summary, we have discussed the implementation of universal gates for trapped-ion quantum information processing (QIP) with oscillating magnetic-field configurations compatible with surface-electrode ion traps. These gates are free of spontaneous-emission decoherence and can be relatively insensitive to motional-state initialization, potentially eliminating the need for near-ground-state cooling. This could enable trapped-ion QIP with the use of rf or microwave fields and relatively low-power optical pumping, Doppler cooling and detection laser beams. The relative absence of phase, intensity, and beam-pointing instabilities that typically accompany laser-induced gates and the high degree of control possible with rf and microwave fields can be an important advantage in increasing the fidelity and reproducibility of gate operations. Given current trap technology, gate durations comparable to those of laser-mediated gates are achievable, with favorable scaling as trap dimensions become smaller. Recent observations of the suppression of anomalous motional heating at low temperatures [17,25] may lead to much smaller dimensions (also not restricted by the diffraction limit on laser beams) and correspondingly higher gate speeds.

*Present address: Lockheed Martin Space Systems Company, Littleton, CO, USA.

[1] J. I. Cirac and P. Zoller, Phys. Rev. Lett. **74**, 4091 (1995).
[2] R. Blatt and D. J. Wineland, Nature (London) **453**, 1008 (2008).
[3] R. Ozeri *et al.*, Phys. Rev. A **75**, 042329 (2007).
[4] D. Leibfried, E. Knill, C. Ospelkaus, and D. J. Wineland, Phys. Rev. A **76**, 032324 (2007).
[5] F. Mintert and C. Wunderlich, Phys. Rev. Lett. **87**, 257904 (2001).
[6] G. Ciaramicoli, I. Marzoli, and P. Tombesi, Phys. Rev. Lett. **91**, 017901 (2003).
[7] M. Johanning *et al.*, arXiv:0801.0078.
[8] D. Leibfried *et al.*, Nature (London) **422**, 412 (2003).
[9] D. J. Wineland *et al.*, J. Res. Natl. Inst. Stand. Technol. **103**, 259 (1998).
[10] H. Dehmelt, Rev. Mod. Phys. **62**, 525 (1990).
[11] J. Chiaverini and W. E. Lybarger, Jr., Phys. Rev. A **77**, 022324 (2008).
[12] K. Mølmer and A. Sørensen, Phys. Rev. Lett. **82**, 1835 (1999).
[13] E. Solano, R. L. de Matos Filho, and N. Zagury, Phys. Rev. A **59**, R2539 (1999).
[14] A. Sørensen and K. Mølmer, Phys. Rev. A **62**, 022311 (2000).
[15] G. J. Milburn, S. Schneider, and D. F. V. James, Fortschr. Phys. **48**, 801 (2000).
[16] S. Seidelin *et al.*, Phys. Rev. Lett. **96**, 253003 (2006).
[17] J. Labaziewicz *et al.*, Phys. Rev. Lett. **100**, 013001 (2008).
[18] D. F. V. James, Appl. Phys. B **66**, 181 (1998).
[19] P. J. Lee *et al.*, J. Opt. B **7**, S371 (2005).
[20] C. Langer *et al.*, Phys. Rev. Lett. **95**, 060502 (2005).
[21] J. Chiaverini *et al.*, Quantum Inf. Comput. **5**, 419 (2005).
[22] D. J. Berkeland *et al.*, J. Appl. Phys. **83**, 5025 (1998).
[23] M. A. Rowe *et al.*, Quantum Inf. Comput. **2**, 257 (2002).
[24] J. J. García-Ripoll, P. Zoller, and J. I. Cirac, Phys. Rev. Lett. **91**, 157901 (2003).
[25] L. Deslauriers *et al.*, Phys. Rev. Lett. **97**, 103007 (2006).